

## A coupled hydrodynamic system of the Lena River delta and the Laptev Sea shelf zone: the model tuning and preliminary results of numerical simulation\*

V.A. Shlychkov, G.A. Platov, A.I. Krylova

**Abstract.** This paper describes a new model of the hydrodynamic system consisting of the Lena River delta and the Laptev Sea shelf zone. The description of a complex fluvial system with many channels, watercourses and estuarine areas is based on the numerical solution of the Saint–Venant equations. The method used is based on the one-dimensional mathematical description of the processes for each segment of the river net and formulation of the coupling conditions for flows at branch points. A scheme adopted here for the interaction with the surrounding areas of the sea shelf implies the unilateral influence of the delta water on the sea currents, i.e., the river is the primary component in the considered system. Preliminary numerical experiments are presented and their results are discussed. With the help of tuning of the model parameters and considering additional physical mechanisms, some possible causes of discrepancies between the results of numerical experiments and observations were identified. The ways of the further improvement of the system of models were outlined and possible problems, that can be efficiently solved, are discussed.

### 1. Introduction

The heat flow of the Lena River is one of the leading climate forcings of the Laptev Sea. The river drains most of north-east Siberia, and its water accumulates heat of southern latitudes and transports it into the sea. The river water passes through the system of distributary network where the main water flow is split to a set of smaller ones with decreasing runoff velocities. The kinematic structure of watercourses thus varies, so the heat flux carried by the river current into the sea, is transformed. At relatively low flow rates typical of the summer–autumn period, the surface heat flux becomes important. It can affect the water temperature especially in shallow parts with a slow flow, causing a variation of the total heat flux related to flows of land waters to the sea. Since the river water significantly affects the ice thermal processes in the Laptev Sea, the spatial distribution of a heat flow

---

\*Supported by Integration Project No. 109 of Siberian Branch of Russian Academy of Sciences.

at the mouth is of considerable interest for the analysis and interpretation of offshore temperature anomalies.

The objective of our paper is to study the dynamics of the river water and the heat flow in the delta of the Lena River to assess their impact on the thermohaline regime of the Laptev Sea by the numerical simulation. The problem is solved by a successive application of the two basic components of the simulation system: a hydrodynamic model of the Lena River delta and a model of water circulation in the Laptev Sea. The interaction of these two components is carried out along the boundary line of the river channels and marine area.

The interaction scheme adopted here implies the unilateral influence of the delta water on the sea currents, i.e., the river is the primary component in the considered system. Theoretical studies of the delta water regime is conventionally related to issues about the distribution of flow between the channels. In the Arctic and Antarctic Research Institute (AARI) a hydraulic method of the water regime calculation in the river deltas was developed [12]. The method does not use the equations of hydrodynamics, but it is an algorithm for solving the problem of the steady water flow in the distributary network based on the transport balance equations for each branching node using hydraulic formulas to describe the river level drop in channels.

The hydrodynamic description of complex fluvial systems is based on the solution to the fluid mechanics equations, closed by means of some assumptions and empirical relationships. A series of published works [1, 22] gave a constructive basis for numerical solutions of the Saint–Venant equations for complex river systems and river mouth areas. The method employed is based on a one-dimensional mathematical description of the processes for each segment of the river net and formulation of the coupling conditions for flows at branch points. In solving the problem in case of a “tree”-type graph, a specially designed factorization method is used for the branched channels systems, while in the case of looping, a guaranteed convergent iteration method is applied.

Currently, theoretical problems of the interaction between the riverine and the marine waters at the mouths of the northern rivers are not understood well. Early mathematical models of the estuarine areas were formulated on the basis of one-dimensional equations describing the processes of longitudinal movement of the river water into the sea and vice versa under the influence of the surge effects [13]. The nature of the estuarine process strongly depends on the morphometric characteristics of the channel, in each channel behaving in different ways. Most of the earlier theoretical studies of the Siberian rivers dealt with river mouths of the estuarine type (Ob, Yenisey). Currently, there are no published works on modeling a complex system of the Lena delta coupled with shelf waters of the Laptev Sea.

## 2. The model of the Lena delta

A mathematical model describes the delta water and thermal regime of the river starting from the gauging station Kyusyur (70.68° N, 127.36° E) in the lower reaches of the Lena River, which offers regular hydrological observations and which can be conditionally considered to be a top point of the delta, down to the confluence of the riverine and the marine waters. The distributary net herein consists of a great set of channels (about 6,000 related streams) and has a complex topology. The creation of the digital terrain model was carried out by vectoring the coastal contours. First, the primary channels were identified among others, as being prominently separate either hydraulically or spatially, and then the secondary channels, playing a subordinate role. The selection criterion was based on the analysis of the width and length of an individual watercourse. The total contribution of small channels was implicitly taken into account by adjusting the widths of the main watercourses, to reach the hydraulic equivalence of the original and the schematized channel structures. On the broad waterways, the main coastline was additionally supplemented with lines orthogonal to the axis of the channel. Such lines gave information specifying the local orientation of the channel as well as the width of a section. Maps and satellite images of the Earth's surface were the original data source for digitizing.

When building a topology map of the delta, each channel along with its individual hydrological characteristics was associated with a directed segment on the plane, and the whole set of these segments formed a connected graph. The nodes of channel branchings correspond to the *vertices* of the graph, and the river areas—to its *edges*. The resulting geometric model of the delta contains a system of 82 linked edges (or channels) and 70 vertices (or branchings). The total length of the graph segments is about 2,500 km. Figure 1 illustrates the structure of the resulting graph. Boundary nodes of the river system are marked with circles with gray shading. The only input node corresponds to the position of gauging station Kyusyur (on edge 1). Other boundary nodes (on edges 4, 11, 16, etc.) are output nodes dividing the riverine and the marine areas.

In order to calculate the volumes of substances transported into the sea, it is necessary to correctly reproduce the redistribution of waters through the channels of the delta. A description of the channels system is based on a hydrodynamic model using the Saint–Venant equations in one-dimensional approximation. For a single stretch of the river with number  $k = 1, 2, \dots, 82$ , momentum and continuity equations have the form [25]:

$$\begin{aligned} \frac{\partial q_k}{\partial t} + \frac{\partial u_k q_k}{\partial s_k} &= -g\omega_k \frac{\partial \zeta_k}{\partial s_k} - \frac{g}{C_s^2 h_k} |u_k| q_k + \frac{b_k \tau_k}{\rho}, \\ \frac{\partial \omega_k}{\partial t} + \frac{\partial q_k}{\partial s_k} &= 0, \end{aligned} \quad (1)$$

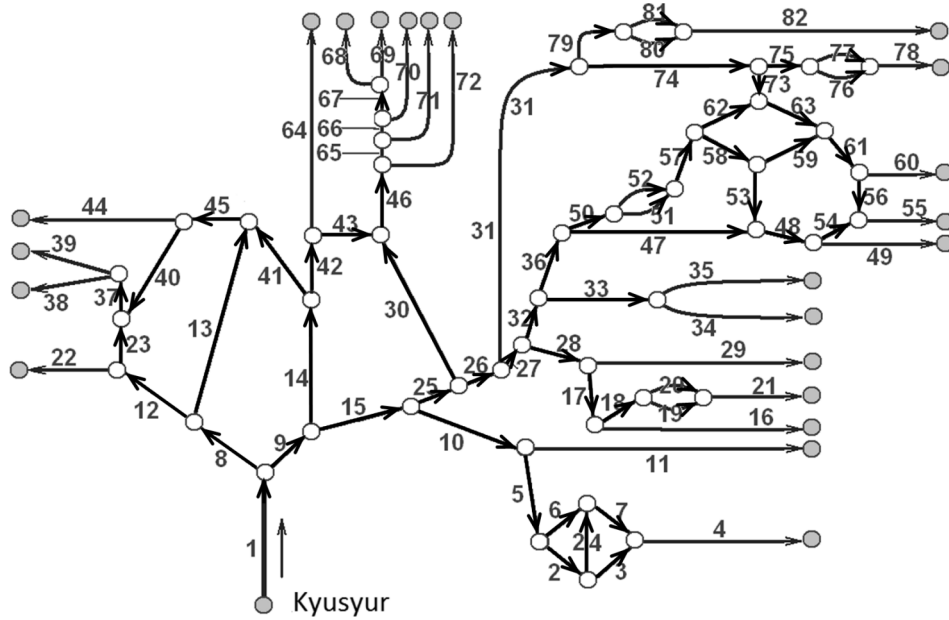


**Figure 1.** Channel network of the Lena delta as a graph. Solid lines (edges) — river watercourses; circles (vertices) — nodes of a branching flow (white) and open boundaries of the graph (gray). The numbers on the edges represent the channel numbering. Arrows indicate the predominant direction of a flow in each channel

where  $s$  is the spatial coordinate that is directed downstream,  $q = u\omega$  is the water transport,  $u$  is the section averaged velocity,  $h$  is the channel depth, defined as the ratio of the section area  $\omega$  to the width of the free surface  $b = \frac{\partial\omega}{\partial\zeta}\Big|_{\zeta=\text{const}}$ ,  $\tau$  is the wind stress,  $\rho$  is the water density,  $C_s$  is the Chézy coefficient characterizing the hydraulic resistance of the channel. All the above variables are to be attributed to the  $k$ th segment.

Let us formulate the boundary conditions for the channel net as a whole. On the input boundary (the edge 1 in Figure 1), the water transport, being supplied from upstream, is assumed to be known

$$q_1 = \bar{q}_1(t), \quad (2)$$

where  $\bar{q}_1(t)$  is the river transport from the observational data. It is assumed that the water elevation at the sea mouth of the river channels coincides with the sea level  $\zeta_0$ :

$$\zeta_k = \zeta_0, \quad (3)$$

where the index  $k$  corresponds to the output nodes of the boundary. In our study, we consider  $\zeta_0 = 0$ .

At internal nodes the continuity of the solution must be ensured. This requires a balance of water transports and level equality at the edges of the

adjacent river sections. For the formulation of internal conditions, note that three edges converge at any available vertex. We denote by  $k_1$ ,  $k_2$ , and  $k_3$  the numbers of these edges. For the sake of definiteness, we assume the edge  $k_1$  to be inflow and the other two edges – outflows at a certain vertex. Then the continuity conditions could be written down as

$$q_{k_1} = q_{k_2} + q_{k_3}, \quad \zeta_{k_1} = \zeta_{k_2} = \zeta_{k_3}. \quad (4)$$

It can be shown that the total number of external (2) and internal (3) boundary conditions corresponds to the orders of the complete system (1), which is a necessary condition for the solvability of the boundary value problem.

The equation of heat within the  $k$ th segment has the form [2]

$$\frac{\partial \omega_k T_k}{\partial t} + \frac{\partial q_k T_k}{\partial s_k} = \frac{\partial}{\partial s_k} \left( \omega_k E_k \frac{\partial T_k}{\partial s_k} \right) + \frac{b_k \Phi_k}{\rho c_p}, \quad (5)$$

where  $T$  is the unknown water temperature,  $E$  is the dispersion coefficient,  $\Phi$  is the surface heat flux. In the absence of sea ice heat flux per unit area is calculated as the sum

$$\Phi = \Phi_s - \Phi_l - \Phi_h - \Phi_e,$$

where  $\Phi_s$  is the absorbed solar radiation,  $\Phi_l$  is the balance of long-wave radiation at the surface,  $\Phi_h$  is a sensible heat flux,  $\Phi_e$  is the latent heat flux due to evaporation. The quasi-stationary boundary layer model based on the Businger unversion functions [4] was used to calculate  $\Phi_h$ - and  $\Phi_e$ -components of the heat flux.

The inflow boundary condition for (5) is taken from the gauge station observations

$$T_1 = \bar{T}_1(t). \quad (6)$$

For the outflows, we imply the zero heat flux condition

$$\frac{\partial T_k}{\partial s_k} = 0. \quad (7)$$

Conditions in the nodes of branching are formulated to balance the horizontal heat fluxes and to preserve the continuity of temperature

$$P_{k_1} = P_{k_2} + P_{k_3}, \quad T_{k_1} = T_{k_2} = T_{k_3}, \quad (8)$$

where  $P = qT - \omega E \frac{\partial T}{\partial s}$ .

The numerical solution of equations (1) is obtained by the method of volume control through the use of an implicit scheme preserving the Bernoulli integral [21]. The finite-difference approximation with a resolution of 500

m was introduced for each river segment. After sampling, the problem was reduced to the solution of algebraic equations for the unknown solution vectors  $\zeta_k$ . Their first and last components are related by (4). The difficulty of solving such problems is that boundary values of the vectors for each segment of the river are not known in advance in the implicit method and must be determined by special methods [26]. At a separate time step, by using a set of parametric factorizations, a decision algorithm reduces to the inversion of a densely filled matrix with the dimension corresponding to the number of vertices of the graph. After determining the boundary elements, the problem is solved by a standard method of factorization. Equation (5) with conditions (6)–(8) can be similarly integrated.

### 3. Morphometric parameters and hydrological information

The model dependence on morphometric characteristics of the river net is realized by specifying the bottom topography  $z_b(s)$  for each channel and the definition of the functional relation

$$\omega_k = \omega_k(s_k, \zeta_k), \quad (9)$$

which allows us to calculate the cross-sectional area as a function of water elevation within the channel area.

The Lena delta, according to its hydrological and morphometric characteristics, applies to complex water bodies. Execution of field work on the vast territory is associated with serious difficulties and therefore is somewhat limited. Currently, the river bed measurements required for the formation of functions in (9), are not complete even for the hydraulically significant watercourses. Only the Bykov outlet has been studied only to the extent necessary for safe navigation, which is undoubtedly not sufficient to describe the delta water body as a whole. For this reason, any source of available, including indirect information, was used to determine the morphometric characteristics of the model. Those were some publications [11, 15, 16], satellite images, data obtained at the international research station “Samoilov island” (126.490° E, 72.374° N) located in the Lena delta.

The bottom topography in the channels was defined after preliminary calculation of the averaged depths along watercourses. For this purpose, for insufficiently studied areas of the delta, hydrological and morphometric relationships statistically established were used. They reflect the dependence of varying watercourse characteristics (depth, cross-sectional area, etc.) on the current river transport. In particular, the expression for the average depth  $h_s$  as a function of the width of the flow follows from the hydrological and morphometric relationships for the Lena watercourses [16] as  $h_s = 0.42b^{0.33}$ . The width  $b$  was calculated according to the digitized map of the channel

net and the value  $h_s$  is used to set the function of the bottom topography by  $z_b = \zeta_s - h_s$ , where  $\zeta_s$  is statistically averaged surface elevation.

The field  $\zeta_s(x, y)$  was built as a continuous function of the horizontal coordinates according to evaluations of the free surface tilt  $\frac{\partial \zeta_s}{\partial s}$  in various parts of the delta [11] and according to the value of  $\zeta_0$ —by the optimization theory methods with smoothing. The field  $\zeta_s$  was used for the calculation of the relief  $z_s$  as well as a base when setting the initial conditions for system (1).

Note that the functions  $\zeta_s$   $h_s$  are introduced here as a helper needed to specify the morphometry at the preliminary stage of the model formulation. Their role is limited to this. The depth  $h$  and the level  $\zeta$  fields are dynamically formed in each cycle of the numerical integration of the basic equations.

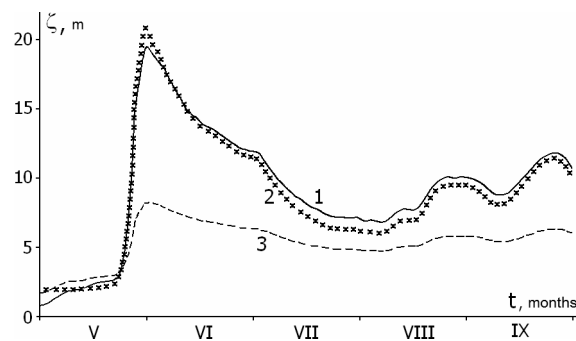
According to [16], the hydrological and morphometric relationships for the Lena River delta determine the function of cross-section geometry (9) as a polynomial of the 4th degree. However, the use of such a relationship in the model has proved to be unsatisfactory due to the formation of a large error when simulating the level regime. Curves 2 and 3 in Figure 2 represent actual and calculated level values at the gauging station Kyusyur. The model values differ from the observed level by 13 m (the seasonal variations of the level are about 19 m), the average error for the period being 3.7 m. Such a large error magnitude indicates to the unacceptability of using relations [16] to define functions (9).

Based on the morphological features of different delta flows (one part of the watercourses has a triangular cross-section shape, the other part is the trapezoid-shaped form [11]), we can assume that dependence (9) is a polynomial

$$\omega_k = A_k h_k + B_k h_k^2,$$

where  $A_k$  and  $B_k$  are coefficients, whose values were determined experimentally for each channel cluster by minimizing the error in the calculated values as compared to the measured ones. These measured values were taken from

**Figure 2.** Progress of the free surface level at the gauge station Kyusyur in 2008: 1—according to calculations, 2—observed, 3—calculated according to hydrological and morphometric relations [16]



observation series at the input boundary (the gauging station Kyusyur). When making a comparison it was taken into account that transport specified on the boundary must coincide with the actual transport  $\bar{q}_1$  according to the boundary condition (2). The levels measured at the gauging station Kyusyur are not used in solving the problem, and the calculated levels are determined in the process of calculation regardless of the actual. The quality of the restored level regime can be derived from the proximity of the calculated and measured values  $\zeta$ . Their closeness proves the adequacy of the overall solution.

Curve 1 in Figure 2 shows the dynamics of the river level at the gauging station Kyusyur, calculated using the model with optimized coefficients  $A_k$  and  $B_k$ . The average absolute error in the determination of  $\zeta_1$  was 0.6 m, which seems acceptable within the accuracy adopted in approximating the riverbed geometry.

While optimizing  $A_k$  and  $B_k$ , the Chézy coefficient values were varied on the river sections in order to achieve the desired proportions in the redistribution of the total flow through the ducts. The data from the literature on the amount of water taken into the river from its basin at different hydrological phases were used in fitting the roughness parameter.

#### 4. The Laptev Sea model with the influence of land waters

A regional model [3], adapted to the Laptev Sea basin with a horizontal resolution concentrated in the vicinity of the delta of the Lena River was used to simulate the marine hydrodynamics. The interaction between global and regional processes is carried out by embedding this model into a global one. The latter includes a large-scale model of the Arctic Ocean and the North Atlantic [7, 8], and a model of the Arctic ice and snow cover [10]. The resulting system of nested models was described in detail in a previous paper [18].

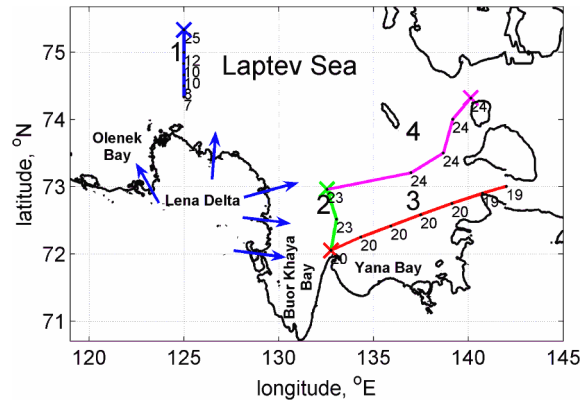
To arrange a river inflow, the position of each channel mouth was chosen so that the smoothed coastal line formed in this place at least 3 grid points in a row, following along the coordinate  $X$  or  $Y$ . This ensures the stability of the boundary conditions for the barotropic velocity  $(U, V)$ , elevation of the sea level  $\eta$ , the temperature  $T$  and the salinity  $S$  in the form

$$\begin{aligned} U = u_k(t) \quad (\text{or } V = u_k(t)), & \quad \frac{\partial \eta}{\partial y} = 0 \quad (\text{or } \frac{\partial \eta}{\partial x} = 0), \\ T = T_k(t), & \quad S = 0, \end{aligned}$$

where  $u_k = \frac{q_k}{\omega_k}$  is the river velocity and  $T_k$  is the water temperature at the mouth of the  $k$ th section of the delta.

The region map indicating the main Lena inflows is displayed in Figure 3.

**Figure 3.** Regional map. Arrows indicate to the main Lena inflows, following clockwise: Olenek, Tumatsk, Trofimof, Sardaksk and Bykov. Lines show the vertical sections to be presented in the following figures. Crosses show the left-most position of the vertical sections. Numbers show the day of September when the IPY measurements were made at each point



## 5. Results

The basic model calculation was carried out using the factual information for 2008, announced by the International Polar Year (IPY). The latter circumstance proved to be important to gain access to databases of Rosgidromet, which carried out an extended programme of hydrometeorological observations in 2008. The calculation is performed for the open-water season from May 1 to October 1. For modeling exchange processes in the surface layer and calculating the components of the heat balance, the NCEP/NCAR re-analysis data were interpolated onto the river and sea grid. These data involve the near-surface wind speed, humidity and temperature of the air, along with precipitation rate and cloudiness. As the initial condition for the model of the river delta, the steady-state solution of the problem was considered with the fixed external and boundary forcing. The initial state of the Laptev Sea was built from the ocean state corresponding to the May 1, 2008 results of the large-scale Arctic and North Atlantic model. This numerical experiment was performed according to the AOMIP rules simulating the period of 1948-2014 (see <http://www.whoi.edu/page.do?pid=29917>).

**5.1. The Lena river delta.** The simulation results of hydrological and thermal regimes of the Lena River from the station Kyusyur and in the downstream are presented in Figures 4 and 5. Figure 4a shows a time series of the total river transport and the contribution of individual watercourses of the Lena River. The lower layers of the presented “pie” are western channels, the upper are eastern. Approximately at 152th day (June 1) the flow reaches a maximum of about  $120,000 \text{ m}^3/\text{s}$ . As for the individual watercourses, a redistribution toward enhancing the contribution of western channels occurs with some weakening of the central and eastern ones. This can be seen from the analysis of Figure 4b, which shows a relative contribution of the main watercourses. Later, there is a tendency to restore the original pattern,

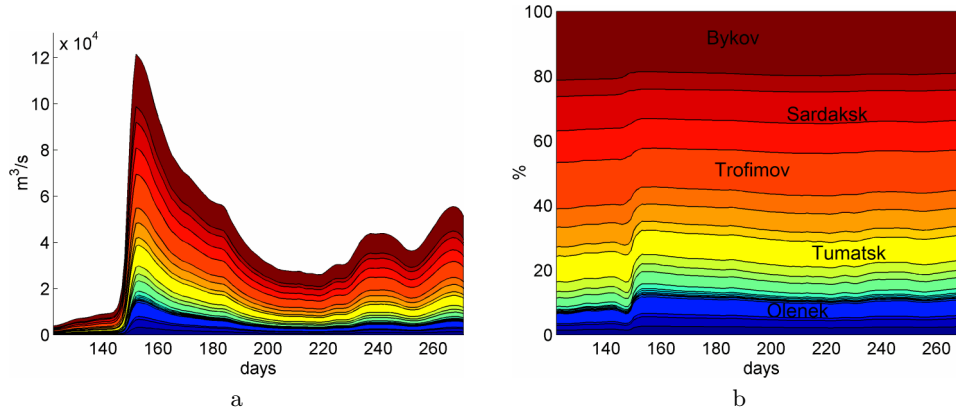


**Figure 4.** Resulting the Lena delta transport to the Laptev sea: a) absolute transport and its distribution among 22 Lena channels; b) a relative distribution among channels. The horizontal axis presents time in days of 2008 (from the 121th day of May 1 until the 274th day of October 1 (no leap years assumed))

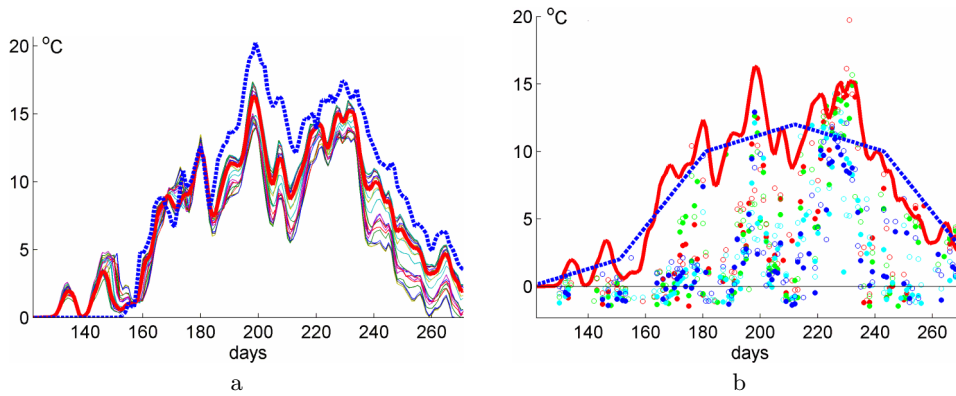


**Figure 5.** The Lena River delta temperature at the entrances to the Laptev Sea: a) resulting from the Lena delta model, thin lines present the distribution of temperature among channels, a bold line is averaged temperature, and a bold dashed line is the original temperature at the gauging station Kyusyur; b) a bold line is the same as above, a dashed line is a piecewise-linear approximation, open and filled circles are day and night satellite estimates of the water temperature in the main Lena channels, blue, cyan, green and red represent Olenek, Tumatsk, Trofimov and Bykov outlets

however the contribution of the Olenek channel still remains increased. The floodwater passage from the gauging station Kyusyur to the mouth is about 1–2 days, resulting in a corresponding delay of the signal.

During May–June–July (days 121–212), the results of observations at the gauging station Kyusyur and the simulation results show the river water heating from zero up to 15–20 degrees Celsius (Figure 5a). And in the lower reaches of the Lena River cooling dominates when moving throughout the riverbed. June (days 152–181) is an exception, during this month the water temperature is almost constant along the river. In August (days 213–243), the water temperature is experiencing slight fluctuations near 13°C, after which there is a noticeable cooling in September. A similar behavior shows the water temperature in the coastal areas of the Laptev Sea, obtained from satellite measurements (Figure 5b). Excluding the synoptic-scale fluctuations, one can obtain a piecewise-linear time dependence of the water temperature in the river:

$$T = \begin{cases} 2(t - 120)/31, & 120 < t < 151, \\ 2 + 8(t - 151)/30, & 151 \leq t < 181, \\ 10 + 2(t - 181)/31, & 181 \leq t < 212, \\ 12 - 2(t - 212)/31, & 212 \leq t < 243, \\ 10 - 8(t - 243)/30, & 243 \leq t \leq 274, \end{cases}$$

where  $t$  is time in days of 2008.

**5.2. The Laptev Sea.** According to results of simulation of the Laptev Sea shelf zone, the distribution of temperature and salinity fields near the river delta is typical of such regions and was considered in a number of publications [5,6,9]. Water discharged from the Lena delta is confined mostly near the delta and the Buor Khaya Bay (see the map in Figure 3) with relatively little freshwater along the coast of the Yana Bay (Figure 6). The surface current is strongest along the boundary between inshore freshwater and offshore saline water, while offshore, the surface velocity is mostly weak.

As normal, during the periods of weak wind forcing, the river plume forms a southward coastally trapped current at the low river discharge or a large recirculating bulge of low-salinity water during a high-discharge event. In the case of a stronger wind forcing, the plume and its velocity field shortly respond to changes in the wind speed direction. Frictional wind-driven currents cause primarily an unidirectional flow down the plume axis to veer to the right or to the left of the axis for south-eastward or north-westward winds, respectively, resulting in a set of meanders, filaments and rings. Farther downstream, currents turn to parallel rather than cross salinity contours, consistent with a geostrophic balance.

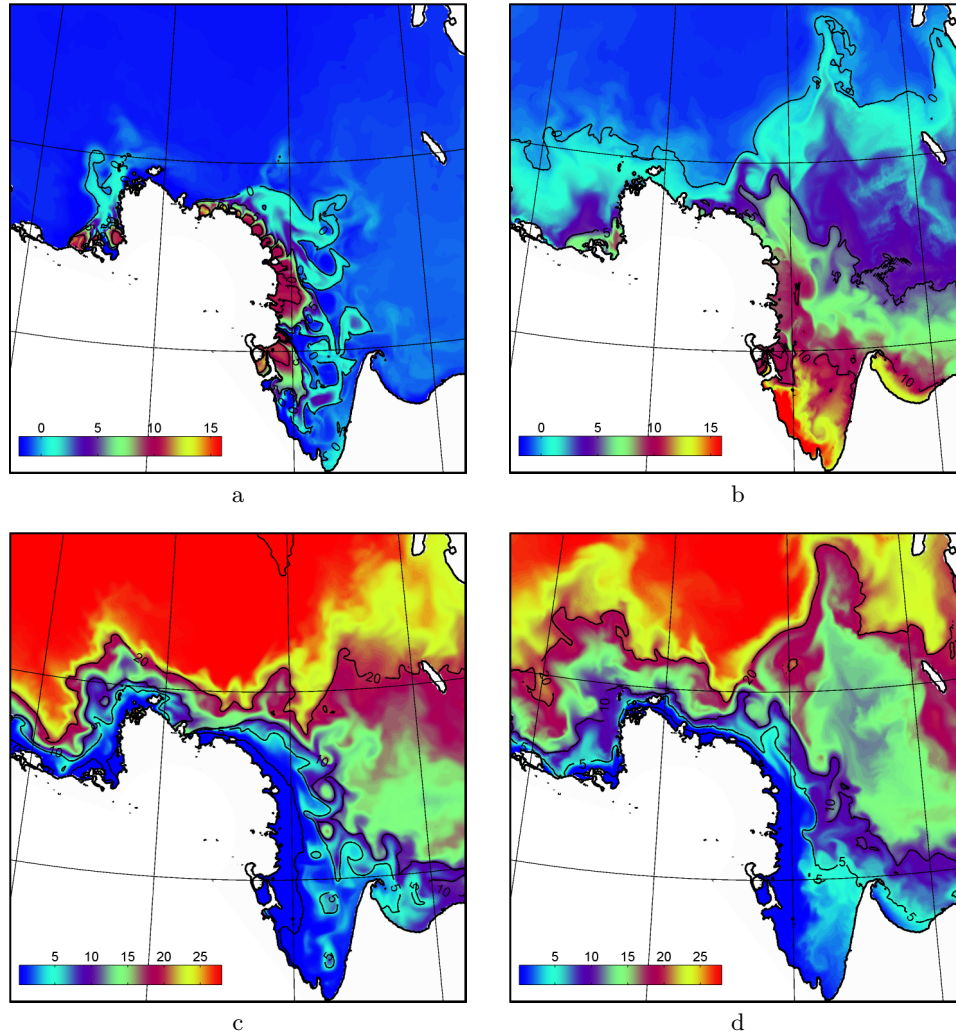


**Figure 6.** The resulting surface temperature (a, b) and salinity (c, d) in the end of June, 2008 at the 180th day (a, c) and in the end of August, 2008 at the 240th day (b, d)

**5.3. Comparison with observational data.** For comparison, we used the vertical sections of the temperature field obtained with the framework of the IPY [20]. The location of the vertical sections is shown in Figure 3. The first one is oriented perpendicular to the shore of the delta and its position meets the northern offshoots of the main stream of the river waters. The second, also perpendicular to the shore, is located north of the Cape Buor Haya and corresponds to the location of the river water penetration from the Buor Haya Bay into the Yana Bay. The third and the fourth vertical sections are oriented along the coastline, demonstrating the vertical

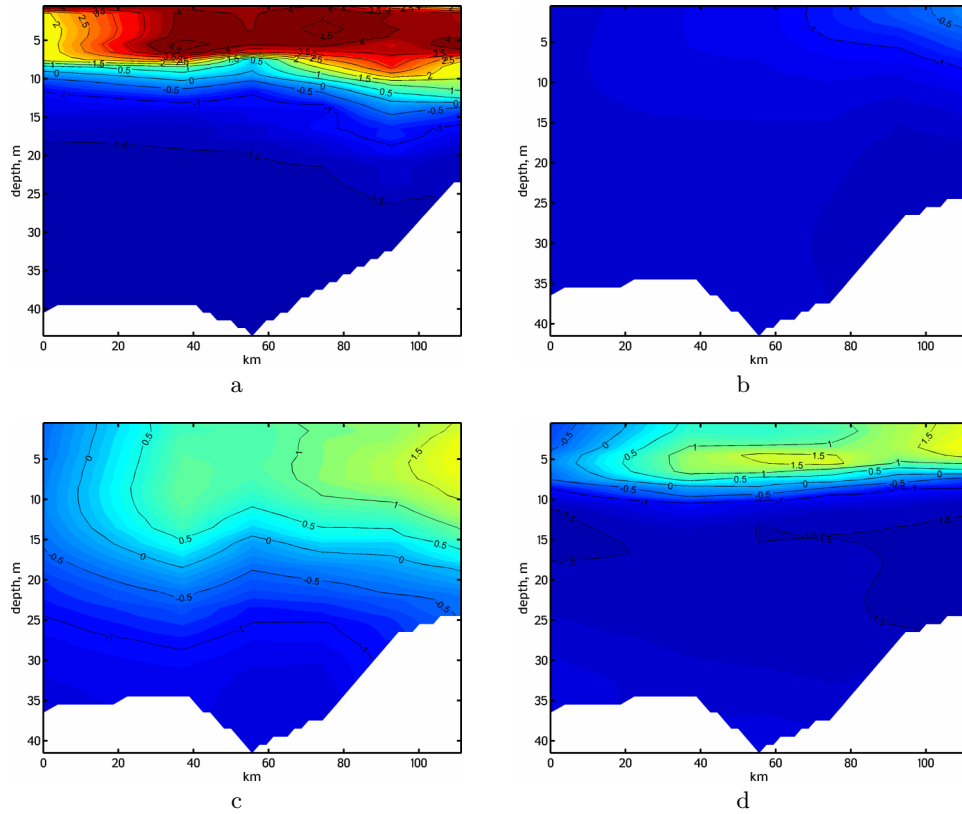


**Figure 7.** Temperature section 1: a) the IPY data, b) a test with the ICMMG model ice distribution, c) a test with the Pathfinder ice distribution, d) the same as c), but with reduced molecular viscosity

structure of waters propagating in the direction of the main straits of the New Siberian Islands.

The first vertical section has the greatest time difference between available measurements. Here a difference between measurements is 18 days. In this regard, we will take the simulated temperature at each point of the vertical section in accordance with the date of corresponding observation. For the remaining vertical sections, the time difference between measurements is unimportant.

The observation results are shown in Figures 7–10, panels (a). The main feature is the well warmed top layer with a temperature of 2–5 °C and a thickness of 10–15 m. Basically, this layer is homogeneous, however, we can distinguish more a colder water on the surface. Figure 7a also shows the presence of a temperature maximum at the lower boundary of this layer. Thickness of the upper layer decreases when moving away from the shore. It can be assumed that such a structure was formed as a result of the summer

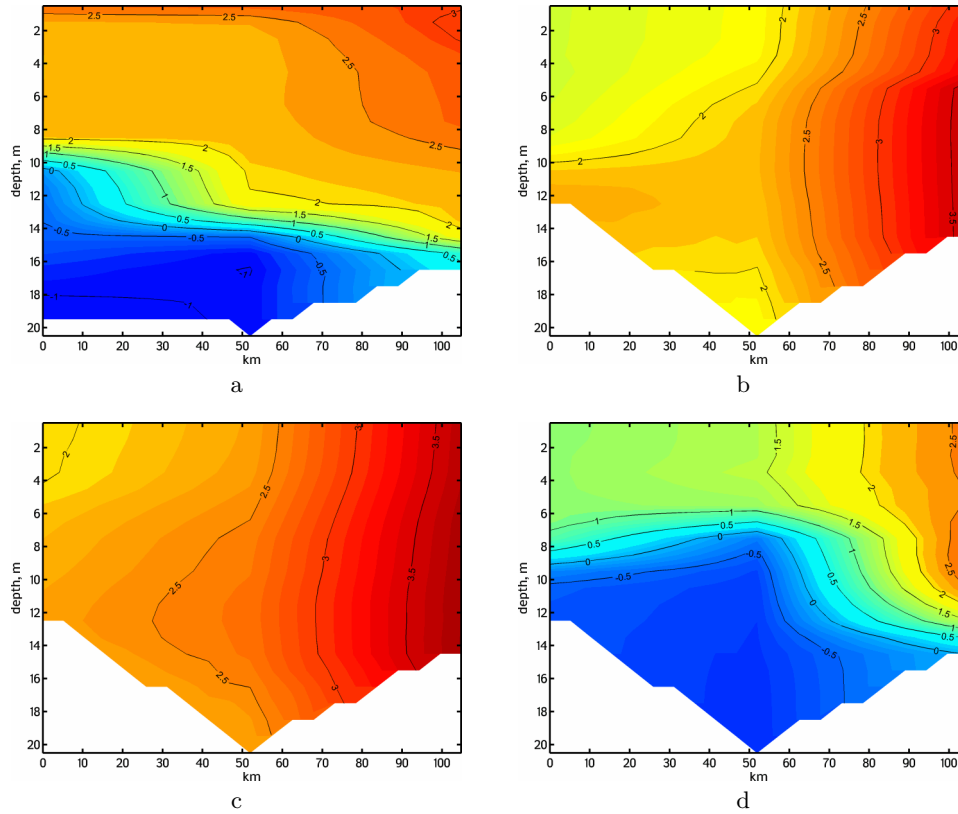


**Figure 8.** Temperature section 2: notations are the same as in Figure 7

warming in combination with wind stirring, followed by the autumn cooling.

This layer is separated with the sharp boundary from the underlying cold layer. The thickness of the transition layer is about 2–5 m. The temperature here has dropped from surface values down to values typical of the Arctic waters,  $-1.5 - -1$  °C. On shallow vertical sections, the depth of these waters corresponds to the bottom hollows.

Alongshore-section off the Yana Bay shows a penetration of waters with temperature of 2.5–3 degrees at the western side of this bay. It is followed by a temperature maximum about the middle of the bay, as well as the next maximum which is located in the alignment of the strait connecting the Laptev Sea to the East Siberian Sea. From this we can assume that the warm riverine water enters the bay at the Cape Buor Haya, and, also, in the middle of the bay after which it is cooled getting inside the bay and then returning back onto this vertical section in the area of the strait with a temperature of 1.5–2 °C. Another version of events leading to this picture is that the water flowing near the Cape Buor Khaya follows along the coast not for long and in the middle of the bay is directed away from the coast

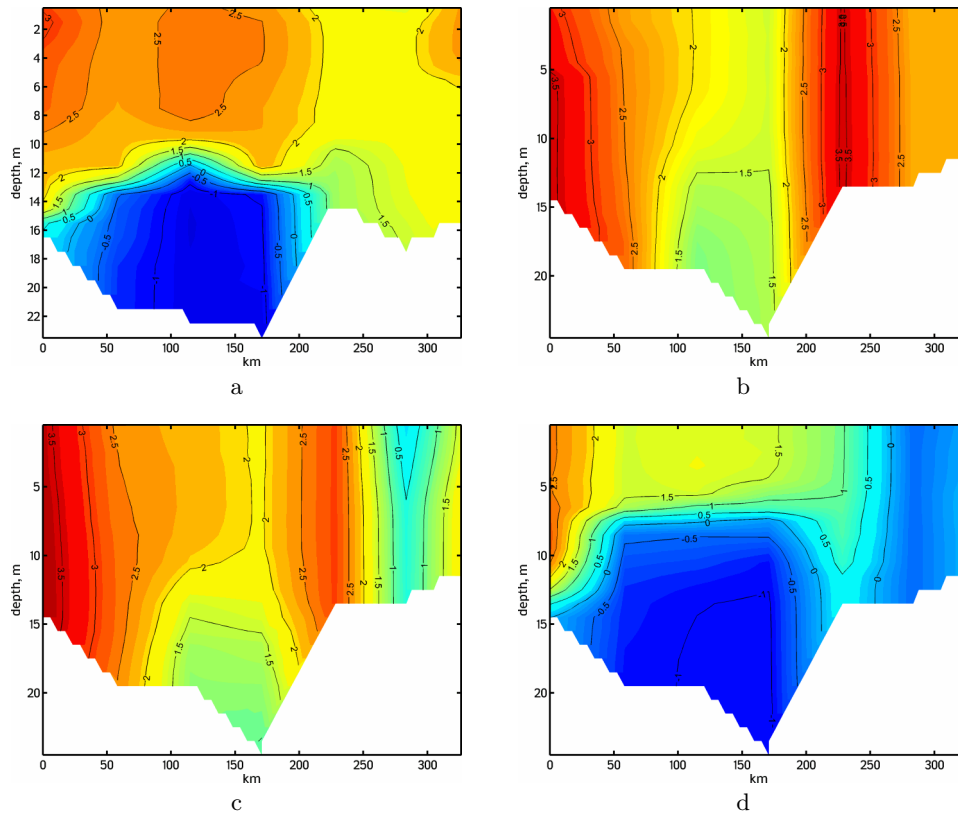


**Figure 9.** Temperature section 3: notations are the same as in Figure 7

and only a small portion of longshore movement continues, reaching strait. Fourth vertical section shows a gradual cooling of the upper water when driving east while increasing the thickness of this layer.

A series of Figures 7–10, panels (b), shows the results of preliminary numerical experiment with a model of the Laptev Sea shelf zone. In general we can say that the main features of the temperature distribution correspond to the observed pattern, however, a detailed comparison shows the following:

- the resulting temperature of the upper layer is significantly lower than that in the first (by 5 degrees) and the fourth (by one degree) vertical sections,
- vertical sections 2 and 3 show that the water, flowing into the Yana Bay near the Cape Buor Haya, is one degree warmer than that observed, its vertical structure is more homogeneous and the upper layer reaches the bottom while it does not in observations,
- the bottom layer of vertical sections 2–4 is somewhat warmer than that in the observations,

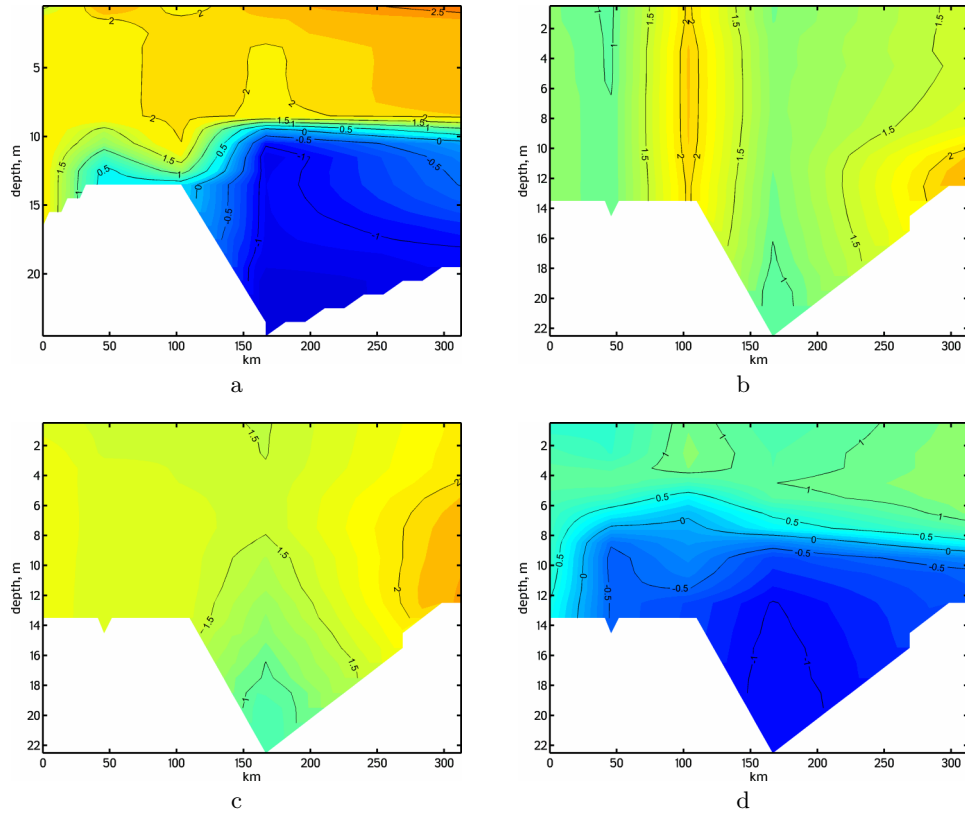


**Figure 10.** Temperature section 4: notations are the same as in Figure 7

- the warm river water, flowing into the Yana Bay, leaves it as a concentrated and vertically uniform jet that can be seen on both the 3rd and the 4th vertical sections, however, this jet is not observed in the data on the 4th section, and on the third it is concentrated in the upper 10 m layer.

**5.4. The model improvements and corresponding results.** A possible explanation of such a strong divergence of the upper layer temperature on the first vertical section is the disparity between the model ice distribution with a really observed pattern. The main differences are that the model distribution does not adequately reproduce:

- the position and intensity of the great Siberian polynya in May 2008,
- reduction in the summer ice area.

Both factors lead to the fact that the model ice distribution isolates the sea water from atmospheric exposure more intensively than in reality. Therefore,

as a step towards improving the results of the numerical calculation it was proposed to keep the real distribution of ice recorded by the Pathfinder satellite measurements (Pathfinder v. 5.3, presented online at the NOAA site).

Figures 7–10, panels (c), presenting the results of this calculation show that due to this we can reduce the temperature difference in the upper layer by 2 degrees. Furthermore, it is seen that the upper layer is deeper (15–20 m) and a transition zone between the upper and the lower layer is more blurred (10–15 m). The character of temperature distribution in the remaining vertical sections did not significantly change. However, a false warm jet in the fourth vertical section has disappeared (although remained on the third one). A correct account of the ice location helps in turning away this jet without reaching the fourth vertical section.

A large mixed layer and a more blurred transition zone indicate to the fact that the background vertical turbulence model is overrated. Therefore, the next step to improve the results of the numerical experiment was in reducing the background turbulent viscosity coefficient from a preliminary experiment value of  $2 \cdot 10^{-5} \text{ m}^2/\text{s}$  down to  $0.1 \cdot 10^{-5} \text{ m}^2/\text{s}$ , i.e., by the factor of 20. The results presented in the figures show the qualitative and quantitative improvement of the restored temperature field as compared to observations for all the considered vertical sections. However, the temperature of the upper layer on the first section is still low, and its thickness becomes even less than the observed one. The same thing is observed when comparing the fourth vertical section.

As a possible cause for such a discrepancy, we considered not quite correct account of the solar radiation, which was accepted in a preliminary experiment. In it, as in the two following experiments, we considered the absorbed solar radiation when forming a heat flux on the ocean surface. Thus, only the upper layer of the model was influenced by the direct solar radiation. This resulted in overheating in the top layer and increasing a sensible heat flux and infrared radiation from the surface of the ocean. Thus, the total heat gain was underestimated. However, in reality the solar radiation penetrates into the deeper layers. The paper [14] shows that the corresponding source can be represented as two exponentials with varying degrees of attenuation for different types of water. In particular, for water with a high content of river ingredients, type III is the most suitable, i.e. the downward flux of the solar radiation is

$$Q_{\text{down}}(z) = Q_{\text{sw}} \left( r \exp\left(\frac{z}{\mu_1}\right) + (1 - r) \exp\left(\frac{z}{\mu_2}\right) \right),$$

where  $Q_{\text{sw}}$  is the downward shortwave radiation at the sea surface,  $r = 0.78$  is a fraction of the total radiance for the first wavelength band,  $\mu_1 = 1.4 \text{ m}$  and  $\mu_2 = 7.9 \text{ m}$  are reciprocals of the absorption coefficient for first and second solar wavelength bands.

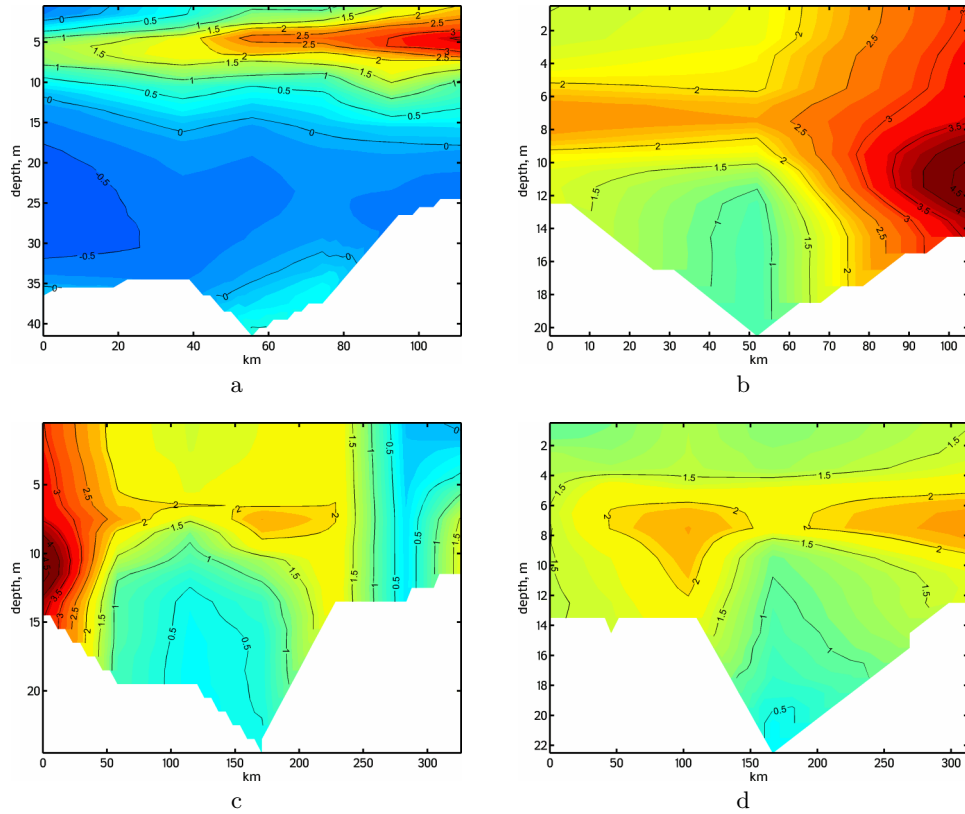


**Figure 11.** Temperature sections 1–4 for experiment with vertically distributed solar radiation flux: a) section 1, b) section 2, c) section 3, and d) section 4.

The result of applying the vertical distribution of the solar flux is shown in Figure 11. From a comparison with the data and with the results of previous experiments, we see that the temperature in the upper layer is closer to the observed temperature and amounts to  $3^{\circ}\text{C}$  in section 1. However, it also increased the temperature of the lower (bottom) layer. According to the observations at depths below 20 m, the temperature was not higher than  $-1.5^{\circ}\text{C}$ , while according to the results of this experiment, the temperature of the layer is  $0 - -0.5^{\circ}\text{C}$ . The same is observed in the other three sections. Furthermore, the surface layer of 0–5 m turned to be supercooled, as compared to available data. Thus, it can be argued that the use of this approach results in a desired increase in the temperature of the upper layer, however, leading to an undesirable warming of underlying layers. The fact that in this experiment, the vertical distribution of temperature significantly changes, indicates that the model is sensitive to the flux parameters of the solar radiation. Further possible steps will be differentiation of the river

and the ocean water transparency, a change in the river water transparency depending on the temperature and flood intensity, with allowance for the diurnal variations of the solar beam direction in the upper ocean. The latter requires some explanation.

The ocean and the river waters differ in their chemical and biological composition, therefore, the transparency of these waters with respect to sunlight is different, i.e., the coefficients  $\mu_1$  and  $\mu_2$  could be different in the previous expression. Therefore, the first thing offered is to calculate the values of these coefficients depending on the concentration of river water for each sea layer; second, to establish a certain empirical dependence of these coefficients on the water temperature and the intensity of river flow. The water temperature determines the biological activity of the plankton, and in the case of an intensive river flow in the process of floods, the river water contains a lot of opaque material washed away from the riverbanks. The last step of improvements is to take into account the angle of the sun rays passing through the upper layer of the ocean. The point is that the exponential distribution of the solar radiation flux does not occur in the vertical direction but in the beam direction. It is important during the day time, since the beam direction changes. Moreover, the considered polar regions are characterized by the low sun above the horizon. With such an inclination of the solar beams, they will scatter more localized in the upper layer, which leads to smaller values for the coefficients  $\mu_1$  and  $\mu_2$  according to

$$\tilde{\mu} = \mu \cos \theta_w,$$

where  $\theta_w$  is the deflection angle of the solar beam from the vertical in sea water. It depends on the angle of incidence on the water surface  $\theta$  by the formula

$$\sin \theta_w = \sin \theta / 1.34.$$

## 6. Discussion

So, we have gained a more acceptable agreement between the calculated temperature field distribution and the observed one as a result of a certain configuration of the model parameters and a more accurate account of the sea ice distribution, as well as by taking into account the vertical distribution of the solar flux. This raises a number of issues that require further discussion. The most common is the question of theoretical interest that is in solving such problems, provided that the practical value of the sea-river system modeling is beyond any doubt. However, in theory, the experiments presented hardly contain any new information for understanding the physical processes in the system. In fact, we only have a practical application of the existing knowledge. Nevertheless, we can offer a number of tasks which

will be interesting both from practical and theoretical standpoints and our coupled model will be an essential tool for solving them.

One of the first tasks is associated with the functioning of the Arctic climate system as a whole. It is known that the atmospheric and the oceanic circulation can be classified using the regional indices. The most important for the Arctic region are indices of the North Atlantic Oscillation (NAO), the Arctic Oscillation (AO) and the Pacific Decadal Oscillation (PDO) [19, 23, 24]. Different values of climatic factors in the study area of the Arctic correspond to specific values of these indices. Analysis of the observations in [17] has shown, for example, the relationship between changes in the average drain of the Siberian rivers and the NAO index in the winter periods from 1936 to 1999, more precisely, the fact that rivers respond to changes in the large-scale circulation of the northern hemisphere. With the help of this model we can investigate the water circulation characteristics in the region, the functioning of the Arctic bio-ecological systems, the biological primary production in the Arctic waters, etc., when implementing a particular set of climate scenarios. In this regard, the development of models of such level is a prerequisite for success.

Another problem is related to environmental monitoring and restoring of real distributions of physical, chemical and biological fields. In this case, as shown by the experiments, we need to involve as much as possible the existing observations, using modern methods of data assimilation. For example, the best available modern ice models are hardly able to reproduce regional ice fields with sufficient accuracy. At the same time, we can regularly get them from satellite data.

In terms of the development of this approach it is an important question: whether we need to take into account the bilateral interaction between the components of the system: the shelf zone of the ocean and the river delta. Each component can function separately and can solve its problems on its own. For example, a model of the shelf zone can directly use the measured river transport at the gauging station Kyusyur, and can set the river water temperature using a linearized approximation shown in Figure 5b. In this paper, we have implemented the approach allowing us to take into account the river runoff volume and physical characteristics of the incoming river water. In its turn the ocean also has an effect on the river delta system which we preliminary neglected. In describing the model of the delta, we have assumed a zero level of water in the channel mouths. However, it can be taken only as the first approximation. The estimates show that the rejection of the zero level does not lead to significant changes. However, the shelf dynamics largely determines the sea level, leading to large variations both in time and space, for example, in a situation with local surges or tidal waves. The movement of river water along certain channels can thus be significantly slowed down or reversed or even accelerated. It still remains

unclear how important it is to consider this interaction.

The importance of integrating the vertical distribution of the solar flux found in the course of experiments, can also be considered only as a preliminary result. The water transparency for different wavelengths depends on many factors and is not obliged to obey a limited set of distributions corresponding to the type of water.

The results of the experiments given in this paper relate solely to the temperature distribution. However, in the regions such as the vicinity of the river delta, the salinity characteristics are much more important. When the salinity changes to one promille, a change in the density of water is four times greater than that in the case of changes in temperature by one degree. In such regions, changes in temperature and salinity are of the same order and make up 1–2 dozens of the corresponding units. The reason why we did not compare the distribution of salinity, is that we cannot use the satellite distribution of ice to obtain the flux of fresh water into the ocean as effectively as in the case with the heat flux. In the case of the heat flux, the fact of whether the water surface is covered with ice or not, is determining, while to produce a fresh water flux it is also important to know the dynamics of its thickness. Such information has not been recorded yet by satellites. There remains the only option, some assimilation of data of ice compactness within the ice model.

## 7. Conclusion

A system of models, including the Lena river delta and the Laptev sea shelf zone, has been developed. Preliminary numerical experiments are presented and their results are discussed. With the help of tuning the model parameters and by considering additional physical mechanisms, some possible causes of discrepancies between the results of numerical experiments and observations were identified. The ways of further improvement of the system of models were outlined and possible problems to be efficiently solved are discussed.

## References

- [1] Atavin A.A., Vasiliev O.F., Voevodin A.F., Shugrin S.M. Numerical methods for solving one-dimensional hydraulic problems // *Water resources.* — 1983. — Vol. 10, No. 4. — P. 47–53 (In Russian).
- [2] Atavin A.A., Zhdanov E.P., Kopylov Ju.N. One-dimensional along-stream model of heat transport and river sedimental deposits in water reservoir // *Meteorol. and Hydrol.* — 1995. — No. 2. — P. 93–101 (In Russian).
- [3] Blumberg A.F., Mellor G.L. 1987. A description of a three-dimensional coastal ocean circulation model // *Three-Dimensional Coastal Ocean Models*, 4 of

- Coastal and Estuarine Series. — Washington, D.C.: American Geophysical Union, 1987. — P. 1–16.
- [4] Businger J.A., Wyngaard J.C., Izumi Y. Fluxprofile relationships in the atmospheric surface layer // *J. Atmos. Sci.* — 1971. — No. 28. — P. 181–189.
- [5] Chant R.J., Glenn S.M., Hunter E., et al. Bulge Formation of a Buoyant River Outflow // *J. Geophys. Res.* — 2008. — Vol. 113. doi:10.1029/2007JC004100.
- [6] Choi B.J., Wilkin J.L. The Effect of Wind on the Dispersal of the Hudson River Plume // *J. Phys. Oceanogr.* — 2007. — Vol. 37, No. 7. — P. 1878–1897. doi:10.1175/JPO3081.1.
- [7] Golubeva E.N., Platov G.A. On improving the simulation of Atlantic water circulation in the Arctic Ocean // *J. Geophys. Res.* — 2007. — Vol. 112. — doi:10.1029/2006JC003734.
- [8] Golubeva E.N., Platov G.A. Numerical modeling of the Arctic Ocean ice system response to variations in the atmospheric circulation from 1948 to 2007 // *Izv. Atmospheric and Oceanic Physics.* — 2009. — Vol. 45, No. 1. — P. 137–151.
- [9] Hickey B.M., Pietrafesa L.J., Jay D.A., Boicourt W.C. The Columbia River Plume Study: Subtidal variability in the velocity and salinity fields // *J. Geophys. Res.* — 1998. — Vol. 103, No. C5. — P. 10339–10368.
- [10] Hunke E.C., Dukowicz J.K. An elastic-viscous-plastic model for ice dynamics // *J. Phys. Oceanography.* — 1997. — Vol. 27, No. 9. — P. 1849–1867.
- [11] Gukov A.Y. Hydrobiology of the Lena River Mouth Area // Moscow: Nauchny Mir, 2001 (In Russian).
- [12] Ivanov V.V. The hydraulic method of water regime elements calculation in river deltas // *Proceedings of AARI.* — 1968. — Vol. 283. — P. 30–63 (In Russian).
- [13] Ivanov V.V., Svyatskiy A.Z. Numerical modeling of sea water intrusion into river mouths at seasonal scales // *Water Resources.* — 1987. — No. 5. — P. 46–51 (In Russian).
- [14] Jerlov N.G. *Optical Oceanography* / Elsevier Oceanography. Series 5. — Elsevier, 1968.
- [15] Korotaev V.N. *Essays on the Geomorphology of the Estuarine and Coastal Systems.* — Moscow: Geographical Faculty of Moscow State University, 2012 (In Russian).
- [16] *Lena Basin Waterways.* — Moscow: MIKIS, 1995 (In Russian).
- [17] Peterson B.J., Holmes R.M., McClelland J.M., et al. Increasing river discharge to the Arctic Ocean // *Science.* — 2002. — Vol. 298, No. 5601. — P. 2171–2173. doi:10.1126/science.1077445.

- [18] Platov G.A. Numerical modeling of the Arctic Ocean deepwater formation: Part II. Results of regional and global experiments // *Izv. Atmospheric and Oceanic Physics*. — 2011. — Vol. 47, No. 3. — P. 377–392.
- [19] Polyakov I.V., Proshutinsky A.Y., Johnson M.A. Seasonal cycles in two regimes of Arctic climate // *J. Geoph. Res.* — 1999. — Vol. 104, No. C11. — P. 25761–25788.
- [20] Scientific program of the Russian Federation participation in the International Polar Year (2007/2008). — Moscow, 2006. — [http://www.ipyrus.aari.ru/scientific\\_program.html](http://www.ipyrus.aari.ru/scientific_program.html).
- [21] Shlychkov V.A. A numerical model for shallow water equations on a curvilinear grid with preservation of the Bernoulli integral // *J. Comp. Math. and Math. Physics*. — 2012. — Vol. 52, No. 4. — P. 1–8 (In Russian).
- [22] Shugrin S.M. Numerical calculation of unsteady water flow in fluvial systems and channels // *Izv. SO AN USSR. Tech. Sci.* — 1969. — Vol. 1, No. 3. — P. 25–31 (In Russian).
- [23] Tompson D.W.J., Wallace J.M. The Arctic Oscillation signature in the winter-time geopotential height and temperature fields // *Geophys. Res. Letters*. — 1998. — Vol. 25, No. 9. — P. 1297–1300.
- [24] Trenberth K., Hurrell J.W. Decadal atmosphere-ocean variations in the Pacific // *Climate Dynamics*. — 1994. — Vol. 9, No. 6. — P. 303–319.
- [25] Vasiliev O.F., Godunov S.K. 1963. Numerical method of long waves in open channels and its application to the problem of high water // *Doklady AN*. — 1963. — Vol. 151, No. 3. — P. 525–527 (In Russian).
- [26] Voevodin A.F., Nikiforovskaya V.F., Ovtcharova A.S. Numerical methods for solving the problem of unsteady motion of water on the estuaries of rivers // *Proceedings of AARI*. — 1983. — Vol. 378. — P. 23–34 (In Russian).

